Imaging of object in the presence of rough surface using scattered electromagnetic field data

Pengju Yang, Lixin Guo, Chungang, Jia

School of science, Xidian University, xi'an 710071, China

***Abstract*-Electromagnetic (EM) scattering from a perfect electrically conducting object above lossy dielectric half-space with rough surface is investigated, for both TE and TM polarizations, employing a parallel fast multiple method. Then, based on the scattered electromagnetic field data at multiple-incidence angles and frequencies, a back-projection tomography technique is applied to generate two-dimensional (2-D) synthetic aperture radar images. The randomly rough surfaces are modeled as realizations of a Gaussian random process with the Gaussian spectrum, while the tapered incident wave is chosen to reduce the truncation error.**

I. INTRODUCTION

The problem of detecting and imaging objects with electromagnetic sensors relies on accurate computational modeling, which is a challenging task duo to the existence of strong ground clutter and low electromagnetic wave penetration into lossy media. Over the past few decades, a significant amount of research effort has been spent toward developing accurate and efficient forward solvers for the scattering problem, which is valid over a wide range of incident and scattering angles. Rigorous numerical methods, such as method of moments (MoM) [1] and its fast algorithms [2] [3] have been implemented to analyze electromagnetic scattering from target embedded in lossy dielectric half-space with a flat interface or rough surface.

A variety of techniques have been provided in recent years to solve this category of problems of the detection of buried objects below rough surface or flat interface. The angular correlation function technique has been applied to the detection of radar object in the presence of rough surface clutters, indicating that ACF technique is more effective than the RCS method in suppressing the clutter due to rough surface scattering effect [4]. Radar imaging techniques have been widely used in the detection of buried targets with the development of wide-band high-resolution synthetic aperture radar (SAR) technology, which has shown its ability to imaging the buried objects. For example, ultra-wideband (UWB) ground penetrating radar (GPR) has been applied extensively to detect the subsurface objects. The radar imaging of target embedded in dielectric half-space has been conducted both theoretically and experimentally [5] [6] [7], which demonstrate the performance of UWB radar in the detection of buried objects.

In this paper, the surface integral equations of scattering problem involving a perfect electric conductor (PEC) object embedded in dielectric media with rough interface formulated by employing Helmholtz equation and Green's theorem. Due to the considerable computation time in tomographic processing which involves the need for data at multiple frequencies and aspect angles, a parallel fast multiple method is applied as a forward solver to solve the surface integral equation. Based on the scattered fields, a back-projection tomography technique is employed to generating SAR images of 2-D cylinder above rough surface.

II. SCATTERING THEORY IMAGEING TECHNIQUE

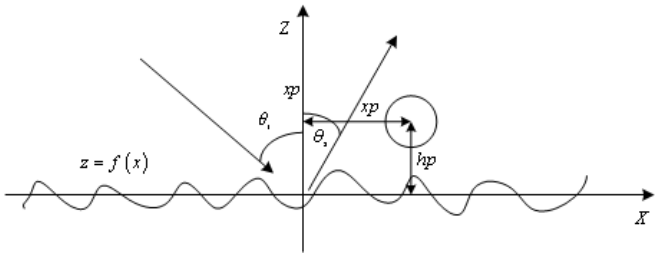

Fig. 1. Geometry of a PEC object above rough surface.

Fig. 1 illustrates the basic geometry considered in this paper: a PEC object is above a rough interface described by $z = f(x)$. The upper medium is vacuum and the lower medium is considered to be lossy with relative complex permittivity ε_1. $\bar{k}_i$ and $\bar{k}_s$ are the incident and scattering wave vector, respectively. θ_i and θ_s are the incident and scattering angle, respectively. *xp* denotes the horizontal distance of between center of the cylinder and the origin, and *hp* represents the height of the object. Let ψ_0 and ψ_1 denote the fields in region 0 and region 1, respectively. Let $\bar{r}' = x'\hat{x} + z'\hat{z}$ and $\bar{r} = x\hat{x} + z\hat{z}$ represent source and field points, respectively.

The randomly rough surfaces are modeled as realizations of a Gaussian random process with the Gaussian spectrum [8]

$$S(k) = \frac{\delta^2 l}{2\sqrt{\pi}} \exp(-k^2 l^2 / 4) \qquad (1)$$

where δ and l are the rms height and correlation length, respectively.

According to Helmholtz equation and Green's theorem, one can obtain the following coupled integrals for the TM case.

$$\begin{aligned}&\frac{1}{2}\psi_0(\bar{r})-PV\int_{S_r}ds'\psi_0(\bar{r}')\hat{n}'\cdot\nabla'G_0(\bar{r},\bar{r}')\\&+\int_{S_r}ds'G_0(\bar{r},\bar{r}')\hat{n}'\cdot\nabla'\psi_0(\bar{r}')\\&-\int_{S_o}ds'\psi_0(\bar{r}')\hat{n}'\cdot\nabla'G_0(\bar{r},\bar{r}')\\&=\psi_{inc}(\bar{r})\qquad \bar{r}\in S_r\end{aligned}\tag{2}$$

$$\begin{aligned}&\frac{1}{2}\psi_0(\bar{r})-\int_{S_r}ds'\psi_0(\bar{r}')\hat{n}'\cdot\nabla'G_0(\bar{r},\bar{r}')\\&+\int_{S_r}ds'G_0(\bar{r},\bar{r}')\hat{n}'\cdot\nabla'\psi_0(\bar{r}')\\&-PV\int_{S_o}ds'\psi_0(\bar{r}')\hat{n}'\cdot\nabla'G_0(\bar{r},\bar{r}')\\&=\psi_{inc}(\bar{r})\qquad \bar{r}\in S_o\end{aligned}\tag{3}$$

$$\begin{aligned}&\frac{1}{2}\psi_1(\bar{r})+PV\int_{S_r}ds'\psi_1(\bar{r}')\hat{n}'\cdot\nabla'G_1(\bar{r},\bar{r}')\\&-\int_{S_r}ds'G_1(\bar{r},\bar{r}')\hat{n}'\cdot\nabla'\psi_1(\bar{r}')=0\quad \bar{r}\in S_r\end{aligned}\tag{4}$$

Note that ψ_{inc} is the incident field. $G_0(\bar{r},\bar{r}')$ is the Green's function in region 0 with $G_0(\bar{r},\bar{r}')=(i/4)H_0^{(1)}(k_0|\bar{r}-\bar{r}'|)$ and $G_1(\bar{r},\bar{r}')$ is the Green's function in region 1 with $G_1(\bar{r},\bar{r}')=(i/4)H_0^{(1)}(k_1|\bar{r}-\bar{r}'|)$, where $H_0^1(\cdot)$ is the zeroth-order Hankel function of the first kind. The aforementioned integral equations can be used for TE polarization with a slight modification.

When $\bar{r}$ is on the rough surface, the total fields satisfy the following boundary conditions

$$\psi_0(\bar{r})=\psi_1(\bar{r})\tag{5}$$

$$\hat{n}\cdot\nabla\psi_1(\bar{r})=\rho\hat{n}\cdot\nabla\psi_0(\bar{r})\tag{6}$$

where $\rho=\varepsilon_1/\varepsilon_0$ for TM incidence, and $\rho=1$ for TE incidence.

To avoid artificial edge diffraction resulting from the finite length of the simulated rough surface, the following Thorso's tapered plane wave rather than the generally used plane wave is chosen as the incident field.

$$\begin{aligned}\psi_{inc}(\bar{r})=&\exp[ik_0(x\sin\theta_i-z\cos\theta_i)(1+w(\bar{r}))]\cdot\\&\exp\left(-(x+z\tan\theta_i)^2/g^2\right)\end{aligned}\tag{7}$$

where g is the tapering parameter controlling the tapering length of the incident wave. The additional factor in the phase is $w(\bar{r})=\left[2(x+z\tan\theta_i)^2/g^2-1\right]/(k_0g\cos\theta_i)^2$.

Upon solving the matrix equation by using a parallel fast multiple method which is based on the message passing interface (MPI), the surface fields and their normal derivatives can be obtained. When the point $\bar{r}$ is located in the far field, the scattered field $\psi^s(\bar{r})$ in space Ω_0 is [8]

$$\psi_s(\bar{r})=\frac{i}{4}\sqrt{\frac{2}{\pi k_0 r}}\exp\left(-i\frac{\pi}{4}\right)\exp(ik_0r)\psi_s^{(N)}(\theta_s)\tag{8}$$

Where

$$\psi_s^N(\theta_s)=\int_{S_1}ds[-i(\hat{n}\cdot\bar{k}_s)I_1(x)-I_2(x)]\exp(-i\bar{k}_s\cdot\bar{r})\tag{9}$$

with $\bar{k}_s=k_0(\sin\theta_s\hat{x}+\cos\theta_s\hat{z})$.

A 2-D SAR image of a deterministic surface can be constructed from a set of frequency and angular swept complex backscatter field data. This corresponds to a "spotlight" SAR image in which the incident beam is oriented to illuminate a fixed surface area. Tomographic processing using an inverse Fourier transform with back projection [9] is employed to generate the images of this paper.

Range and cross-range resolutions of the image can be determined by the frequency and angular bandwidths, respectively. The range and cross-range resolutions, r_d and r_c, are given by

$$r_d=\frac{c}{2B}\qquad r_c=\frac{c}{2f_0\sin\theta}\tag{10}$$

where c is the velocity of light, and B and θ represent the frequency bandwidth centered on f_0 and the angular rotation, respectively. To resolve surface variations on the order of a wavelength, backscatter data were collected over a 4GHz frequency bandwidth (3-7GHz) and a 40° angular bandwidth corresponding 3.75cm range and 4.67cm cross-range resolution in the image domain, respectively.

The unambiguous range and cross-ranges, D_d and D_c, can be obtained by the following equations

$$D_d=\frac{c}{2\delta f}\qquad D_c=\frac{c}{2f_0\delta\theta}\tag{11}$$

where δf and $\delta\theta$ denote the steps in frequency and angle, respectively.

To reduce the side-lobe level, a proper choice of windows is necessary. Since image formation is closely related to the Fourier transform, there is a tradeoff between side-lobe level and spatial resolution. Windows functions in both frequency

and angle are chosen to set the relationship between these quantities. A rectangular window has optimum resolution, but the first side-lobe level is relatively high (-13 dB) so that minor scattering events other than strong single scattering can be completely obscured by the side lobes. The Hamming window has a low side-lobe level (-43 dB) with a wider main lobe. The disadvantage of the Hamming window is that the side-lobe level does not decrease significantly at wide ranges. Throughout this paper a Blackman window is selected as an appropriate choice for the windowing function, resulting in a fast decaying side-lobe level at the expense of degrading image resolution.

III. Numerical Results and Discussions

First, one investigate the spot-mode SAR images of the deterministic Gaussian rough surface of length $L = 2.2\,\mathrm{m}$ with correlation length $l = 12.8\,\mathrm{cm}$ and rms $\delta = 1.3\,\mathrm{cm}$. Fig. 2 shows the radar images constructed from Kirchhoff approximation backscattered prediction for both TE and TM polarization. Each image is expressed within the dynamic range of 60 dB ($-60\,\mathrm{dB} \sim 0\,\mathrm{dB}$) and composed of 200×200 pixels in range $2.2\,\mathrm{m}\times2\,\mathrm{m}$ so that each pixel size is much smaller than the range resolution. The pixel resolution depends on the choice of windowing function as well as the angular and frequency bandwidths. It is observed that the scattering centers are on the entire domain of rough surface due to the plane wave illumination on the rough surface rather than concentrating on the center of the rough surface resulting from the tapered wave illumination. The radar images for both TE and TM polarization exhibit similar distribution of scattering centers show little polarization dependence.

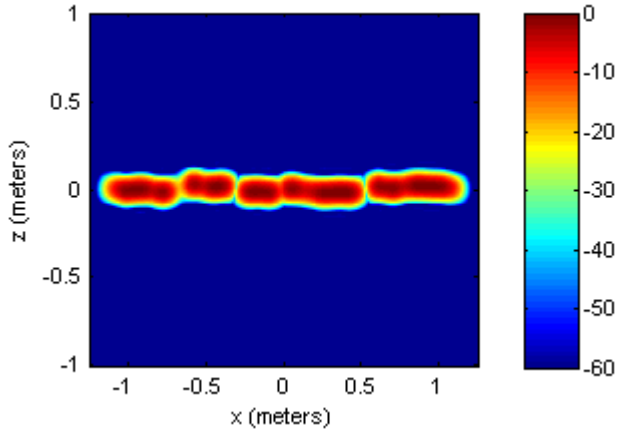

(a)

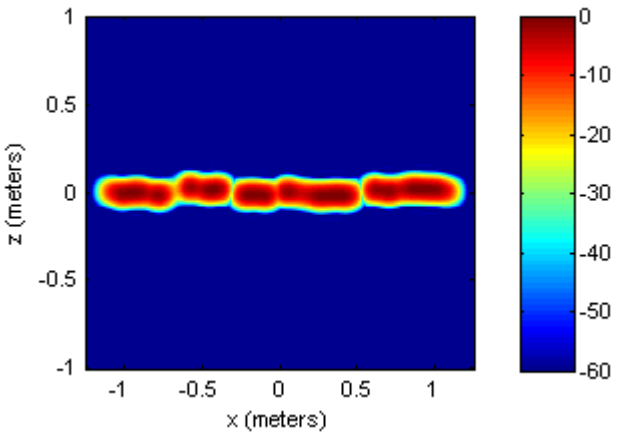

(b)

Fig. 2. Radar images of Gaussian rough surface. (a) TE (b) TM

Fig. 3 exhibit the radar image of object above rough surface for both TE and TM polarization, in which the Blackman window is utilized. The length of the rough surface is $L = 1.98\,\mathrm{m}$ with correlation length $l = 7.5\,\mathrm{cm}$ and rms $\delta = 1.25\,\mathrm{cm}$. The position parameters of the object is $xp = 0.0\,\mathrm{m}$, $hp = 0.3\,\mathrm{m}$ and the radius of the cylinder is $R = 0.1\,\mathrm{m}$. The images are expressed within the dynamic range of 40 dB ($-40\,\mathrm{dB} \sim 0\,\mathrm{dB}$) and composed of 200×200 pixels in range $2\,\mathrm{m}\times2\,\mathrm{m}$ so that each pixel size is much smaller than the range resolution. The object can be clearly observed in the presence of rough surface which will result in clutter and obscure the object. It is readily found that scattering centers are at the central domain which is attributed to the taperd wave illumination, while the scattering centers are distributed on the entire domain of rough surface resulting from the plane wave illumination as depicted in Fig. 2.

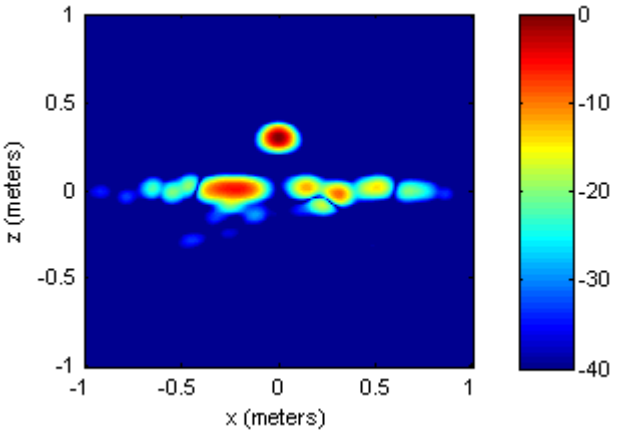

(a)

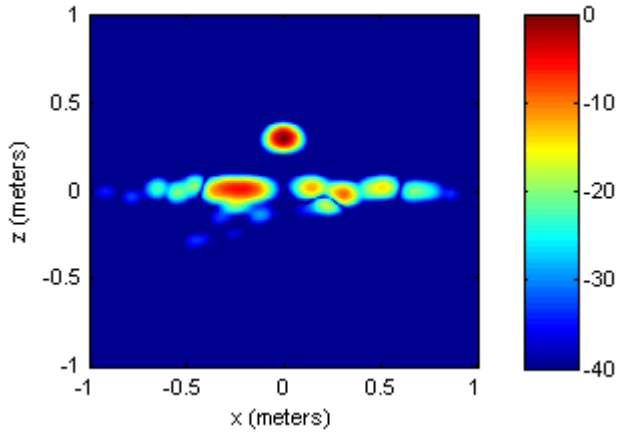

(b)

Fig. 3. Radar images for different polarization. (a) TE (b) TM

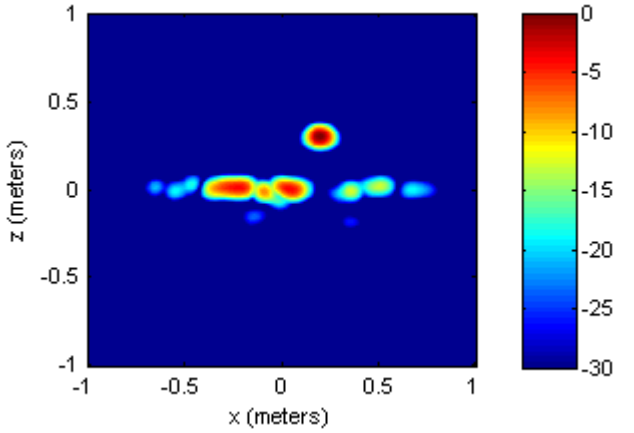

(a)

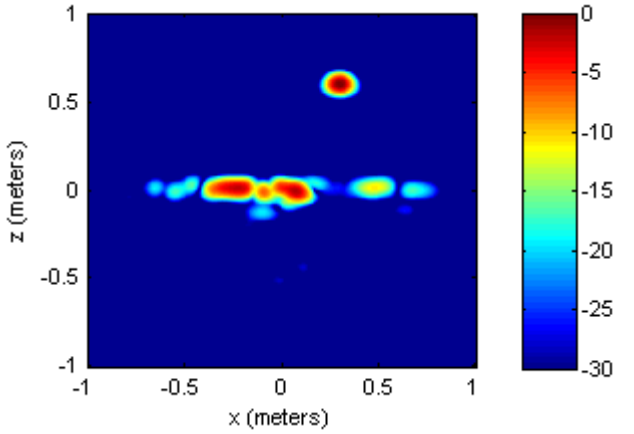

(b)

Fig. 4. Radar images with different object positions.

Fig.4 present the radar image of object with different positions in the presence of rough surface, and the incident wave is TM polarization. The Blackman window is utilized in all the following results. In Fig. 4(a), the position parameters of the object is $xp = 0.2\,\mathrm{m}$, $hp = 0.2\,\mathrm{m}$ and the radius of the cylinder is $R = 0.1\,\mathrm{m}$, and in Fig. 4(b) the position parameters of the object is $xp = 0.2\,\mathrm{m}$, $hp = 0.3\,\mathrm{m}$. The radius of the cylinder is $R = 0.1\,\mathrm{m}$ in Fig. 4. It is readily observed that the position of the object is different from the one in Fig. 3.

IV. Conclusion

In this paper, mono-static radar images of 2-D composite model involving an object above rough surface have been investigated. A parallel fast multiple method is applied as a forward solver to solve the composite electromagnetic scattering problem. Based on the scattered fields, a back-projection tomography technique is employed to generating SAR images of 2-D cylinder above rough surface. The results show that radar images for both TE and TM polarization can be obtained. The studies of this paper demonstrate that radar images provide a means for better understanding of composite scattering problems

Acknowledgment

This work was supported by the National Science Foundation for Distinguished Young Scholars of China (Grant No. 61225002), the Specialized Research Fund for the Doctoral Program of Higher Education (Grant No. 20100203110016), and the Fundamental Research Funds for the Central Universities (Grant No. K50510070001). The authors would like to thank the reviewers for their helpful and constructive suggestions.

References

[1] J. T. Johnson and R. J. Burkholder, "A study of scattering from an object below a rough surface," *IEEE Transactions on Geosciences and Remote Sensing,* vol. 42, pp. 59-66, 2004.

[2] N. Geng, A. Sullivan, and L. Carin, "Fast multipole method for scattering from an arbitrary PEC target above or buried in a lossy half space," *IEEE Transactions on Antennas and Propagation,* vol. 49, pp. 740-748, 2001.

[3] L. Yu, G. Li-Xin, and W. Zhen-Sen, "The fast EPILE combined with FBM for electromagnetic scattering from dielectric targets above and below the dielectric rough surface," *IEEE Transactions on Geosciences and Remote Sensing,* vol. 49, pp. 3892-3905, 2011.

[4] G. Zhang and L. Tsang, "Application of angular correlation function of clutter scattering and correlation imaging in target detection," *IEEE Transactions on Geosciences and Remote Sensing,* vol. 36, pp. 1485-1493, 1998.

[5] A. Sullivan, R. Damarla, N. Geng, Y. Dong, and L. Carin, "Ultrawide-band synthetic aperture radar for detection of unexploded ordnance: modeling and measurements," *IEEE Transactions on Antennas and Propagation,* vol. 48, pp. 1306-1315, 2000.

[6] L. Lin, A. E. C. Tan, K. Jhamb, and K. Rambabu, "Buried Object Characterization Using Ultra-Wideband Ground Penetrating Radar," *IEEE Transactions on Microwave Theory and Techniques,* vol. 60, pp. 2654-2664, 2012.

[7] I. Catapano, L. Crocco, Y. Krellmann, G. Triltzsch, and F. Soldovieri, "A Tomographic Approach for Helicopter-Borne Ground Penetrating Radar Imaging," *IEEE Geoscience and Remote Sensing Letters,* vol. 9, pp. 378-382, 2012.

[8] L. Tsang, *Scattering of Electromagnetic Waves: Numerical Simulations* vol. 2. New York: Wiley-Interscience, 2001.

[9] D. C. Munson, Jr., J. D. O"Brien, and W. Jenkins, "A tomographic formulation of spotlight-mode synthetic aperture radar," *Proceedings of the IEEE,* vol. 71, pp. 917-925, 1983.